CrossMark

Phosphate and Borate Ions as Inhibiting Agents for Cu–10Al–10Zn Corrosion in Saline Solution

H. Nady[1,2] · M. El-Rabiei[1] · M. Samy[1]

Abstract In this article, the inhibitive effects of di-sodium borate and tri-sodium phosphate on the Cu–10Al–10Zn alloy corrosion in NaCl solutions are investigated. Polarization techniques and electrochemical impedance spectroscopy (EIS) were used. Surface examination and morphological studies were employed. All investigations were carried out in stagnant naturally aerated neutral 3.5% NaCl solution containing different concentrations of PO_4^{3-} and $B_4O_7^{2-}$ ions. Polarization measurements reveal that phosphate and borate ions have the large effect on the corrosion current density of Cu–10Al–10Zn in 3.5% NaCl solution. As PO_4^{3-} concentrations increase, the current density decreases till 0.05 M PO_4^{3-} and starts to increase again in contrast to $B_4O_7^{2-}$ where the latest amount (0.01 M) decreases the current density to its minimum value and then increases as $B_4O_7^{2-}$ concentration increased. EIS measurements have shown that a more resistive passive film is formed on the Cu–10Al–10Zn alloy in the presence of PO_4^{3-}. The formation of such passive film on the alloy surface was discussed. The impedance data were fitted to equivalent circuit model that explains the different electrochemical processes occurring at the electrode/electrolyte interface.

✉ H. Nady
  nhm00@fayoum.edu.eg; nhmahmod@ju.edu.sa

[1] Chemistry Department, Faculty of Science, Fayoum University, Fayoum, Egypt

[2] Chemistry Department, Faculty of Science and Arts in Qurayate, Al Jouf University, 2014, Sakaka, Saudi Arabia

 Springer

Graphical Abstract Phosphates and borates can be considered as effective corrosion inhibitors for the corrosion of Cu–10Al–10Zn alloy in 3.5% NaCl solution

corrosion rate to obtain the appropriate results, especially, of metals and alloys which are present in contact with aggressive environments. Accordingly, corrosion inhibitors
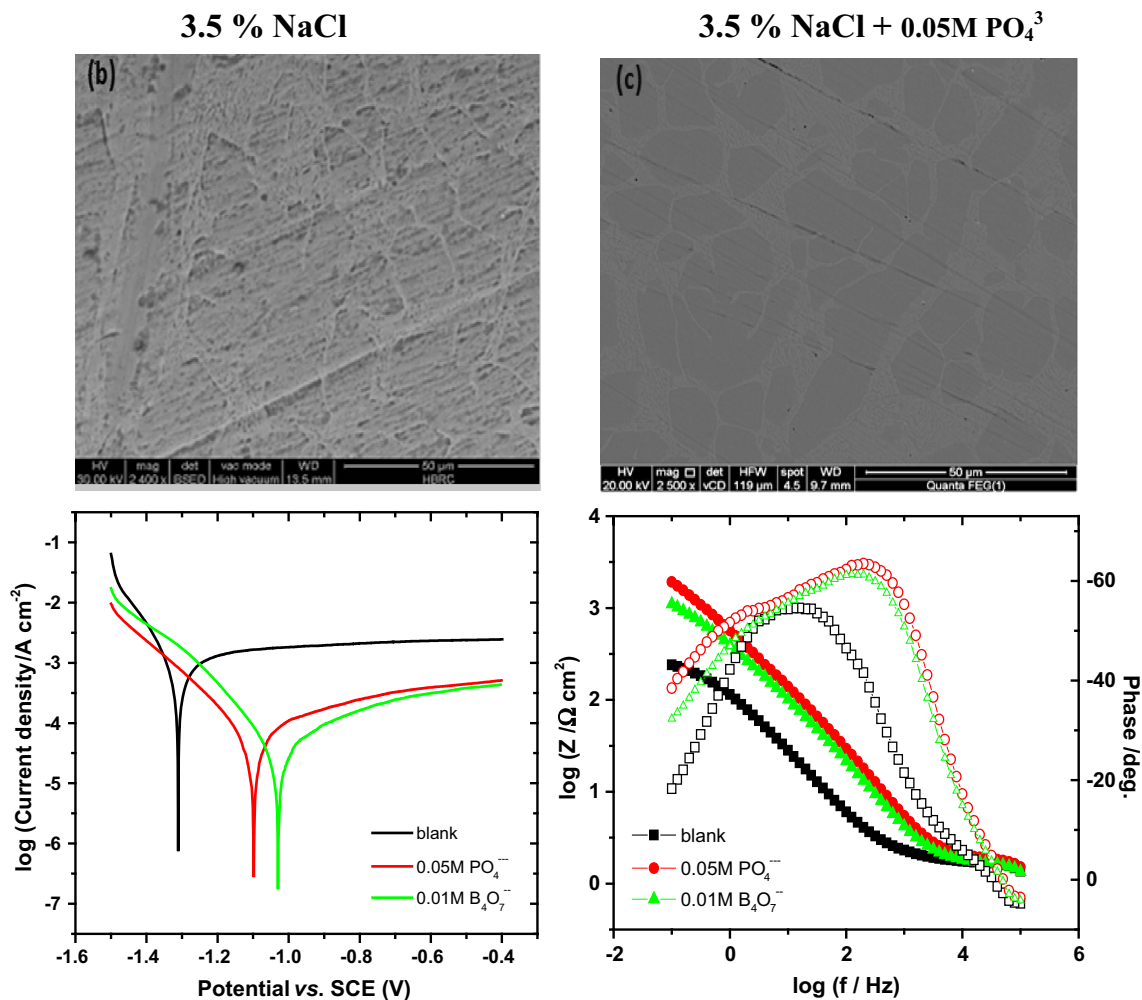
3.5 % NaCl

3.5 % NaCl + 0.05M PO$_4^3$

1 Introduction

The corrosion behavior of metals and alloys in corrosive media depends on many factors such as the chemical composition, stability of the oxide film, and the effectiveness of any applied protection [1]. Alloying of Cu with other elements (e.g., Zn, Al) leads to the formation of alloys, such as Cu–Al–Zn, with improved mechanical properties and higher corrosion resistance. Such alloys are used extensively for condenser tubes and tube sheets in heat exchangers in power plants, oil refineries, and chemical plants. Sometimes, alloying of Cu not controlled to the

are widely used to reduce the corrosion rate of Cu alloys. The addition of inhibitors remains one of the most necessary procedures used to protect metals and alloys against attack in many industrial environments [2]. The use of inorganic inhibitors is one of the most practical and effective methods for metal and alloy protection [3]. These inhibitors should be innocuous for human consumption and they should not have a negative impact on the environment. Among these inorganic additives, tri-sodium phosphate (TSP) has been studied as an inhibitor for brass for several decades [3–13]. Ashour and Ateya [14] have shown that dihydrogen orthophosphate (DHP), inhibits the SCC of brass in nitrite solutions, which is attributed to the formation of zinc phosphate on the surface of the alloy which inhibits dezincification. Valcarce et al. [13, 15, 16] studied the effect of phosphate ions on brass exposed to tap water

and concluded that the presence of phosphate ions inhibited the dissolution of brass due to the formation of a zinc phosphate layer on the brass surface. In fact, due to the beneficial effect of phosphate ions on copper in different tap waters, they are well established as efficient inhibitors for general corrosion of copper compositions, which has been studied by many authors [17–20]. It has been suggested that it lowers copper solubility, forming a cupric phosphate layer on the copper surface [11, 17]. Also, Feng et al. found a synergistic inhibitory effect of tri-polyphosphate compounds on copper when zinc ions are present in tap water [21]. In addition, when phosphate ions are present in high concentrations, a delay in the onset of the anodic dissolution process on brass has been attributed to the development of a zinc phosphate layer [14, 22].

With respect to the environment, di-sodium tetra-borate (borax) is characterized by a stable pH in the bulk and at the electrode surface that provides stable corrosion conditions. In the meanwhile, borate solution is widely used in the oxidation process of magnesium alloys [23, 24], because it can promote the growth of oxide film by rapidly decomposing $B_4O_7^{2-}$ anion and providing oxygen to a metal cation under the effect of an electric field. Undoubtedly, borates as well as phosphates are very commonly used as suitable additives to facilitate the formation of protective films on alloy surfaces [23, 25]. Although the fact that borate ions possess an inhibitive effect on copper alloys cannot be sidelined, as estimated in this research, there are very few papers that deal with this purpose. So that the aim of this work is to study and characterize the corrosion and passivation properties of Cu–10Al–10Zn alloy in aqueous tri-phosphate and tetra-borate solutions. The materials were found to be good inhibitors for Cu–Al–Zn alloy corrosion in chloride-containing solutions. Also the effect of each species on the pitting potential and its passivation and protection will be evaluated in 3.5% NaCl solution which simulates seawater. These measurements were performed using different techniques, including open circuit potential (OCP), linear sweep voltammetry, polarization curves, electrochemical impedance spectroscopy (EIS), which were complemented by SEM examination.

2 Experimental Details

2.1 Electrode Preparation

The working electrode was made of commercial grade Cu–10Al–10Zn rod prepared in our metallurgical workshop. The prepared alloy was cast without any special treatment. The metallic rods were mounted into glass tubes by two-component epoxy resin leaving a surface area of 0.2 cm^2 to contact the solution. The chemical composition of the alloy (Cu–10Al–10Zn) in mass percent is 79.14 Cu, 10.40 Al, 10.20 Zn, 0.01 Ni, 0.01 Mn, 0.02 Sn, 0.21 Fe, 0.01 Si, and 0.01 Mg.

2.2 Electrochemical Cell and Surface Pretreatment

The electrochemical cell is a three-electrode all-glass cell, with a platinum spiral counter electrode for connection and saturated calomel electrode (SCE), as a reference electrode. Prior to each experiment, the working electrode was polished using successive grades of emery papers down to 2500 grit, and then the electrode was rinsed gently with demineralized water and transferred quickly to the electrolytic cell.

2.3 Electrolyte Composition

All solutions were prepared using analytical grade reagents and demineralized water. Experiments were carried out in 3.5% NaCl solutions in the absence and the presence of various concentrations of tri-sodium phosphate (TSP), (Na_3PO_4) and di-sodium tetra-borate, borax, $(Na_2B_4O_7)$. All the experiments were carried out at room temperature (25 °C) in stagnant, naturally aerated alkaline solutions of pH 9.5. Before each experiment, the pH of the solution was controlled by adding few drops of 0.1 M NaOH solution and checked by the sensitive pH meter.

2.4 Electrochemical Techniques

The potential of the working electrodes under the open circuit conditions was measured separately against the saturated calomel $(Hg/Hg_2Cl_2/Cl_{sat}^-)$ reference electrode [$E^o = 244$ mV vs. the standard hydrogen electrode (SHE)]. The open circuit potential (OCP), was recorded after 60 min of electrode immersion. Also potentiodynamic polarization experiments and electrochemical impedance spectroscopic investigations were performed. Both techniques were performed using a VoltaLab PGZ 100 "*All-in-one*" Potentiostat/Galvanostat. The potentials were measured against and referred to as the standard potential of the SCE. To achieve quasi-stationary condition, the polarization experiments were carried out using a scan rate of 10 mV s^{-1}. The total impedance, Z, and phase shift, θ, were measured in the frequency range from 0.1 to 10^5 Hz. The superimposed ac signal peak-to-peak amplitude was 10 mV as assigned by the measuring system.

3 Results and Discussion

3.1 Open Circuit Potential Measurements

The variation of OCP for Cu–10Al–10Zn alloy with time in 3.5% NaCl solution in the absence and the presence of 0.05 M Na_3PO_4 and 0.05 M $Na_2B_4O_7$ at pH 9.5 is

presented in Fig. 1a. During the first 10 min of immersion, the OCP moves sharply toward more negative values and then stabilized to achieve the steady-state potential, usually about 30 min after immersion. As explained, the presence of 0.05 M Na_3PO_4 and 0.05 M $Na_2B_4O_7$ shifts the steady-state potential to less negative values, where the corrosion potential recorded in the presence of 0.05 M PO_4^{3-} is more positive than that recorded for $B_4O_7^{2-}$. This means that the electrode surface is subjected to more passivation processes in the presence of PO_4^{3-} than in the presence of $B_4O_7^{2-}$ as will be confirmed by the polarization and impedance measurements. Figure 1b shows the evolution of OCP for Cu–10Al–10Zn alloy immersed in 3.5% NaCl solution in the absence (blank) and presence of various concentrations (0.01–0.2 M) of PO_4^{3-} ions. The addition of PO_4^{3-} at different concentrations shifts the steady-state potential toward more negative values, indicating that the alloy surface becomes more passive at lower concentrations.
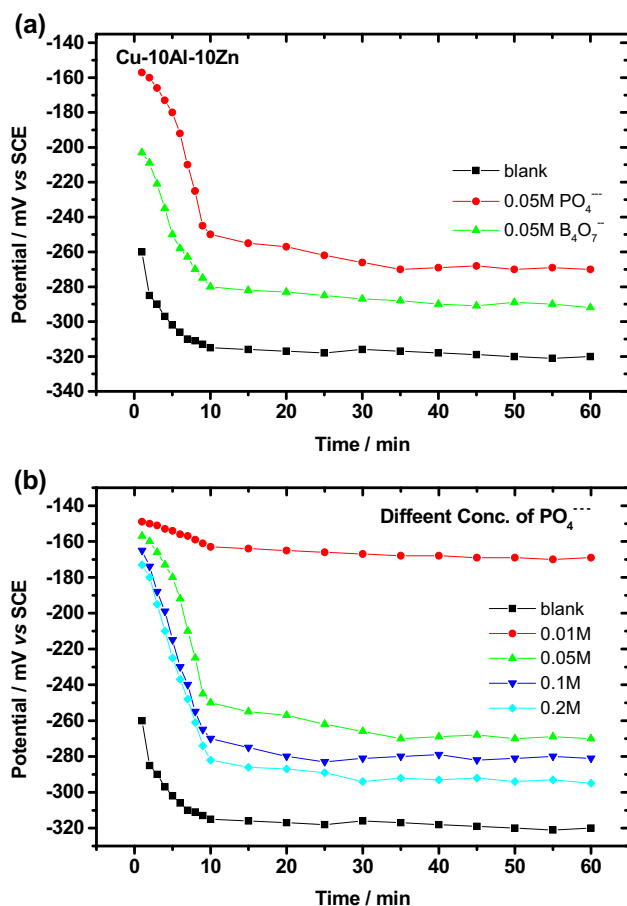

Fig. 1 **a** Variation of OCP for Cu–10Al–10Zn alloy with time in 3.5% NaCl solution in the absence and the presence of 0.05 M Na_3PO_4 and 0.05 M $Na_2B_4O_7$ at 25 °C. **b** Variation of OCP for Cu–10Al–10Zn alloy with time in 3.5% NaCl solution in the absence and the presence of different concentrations of PO_4^- at 25 °C
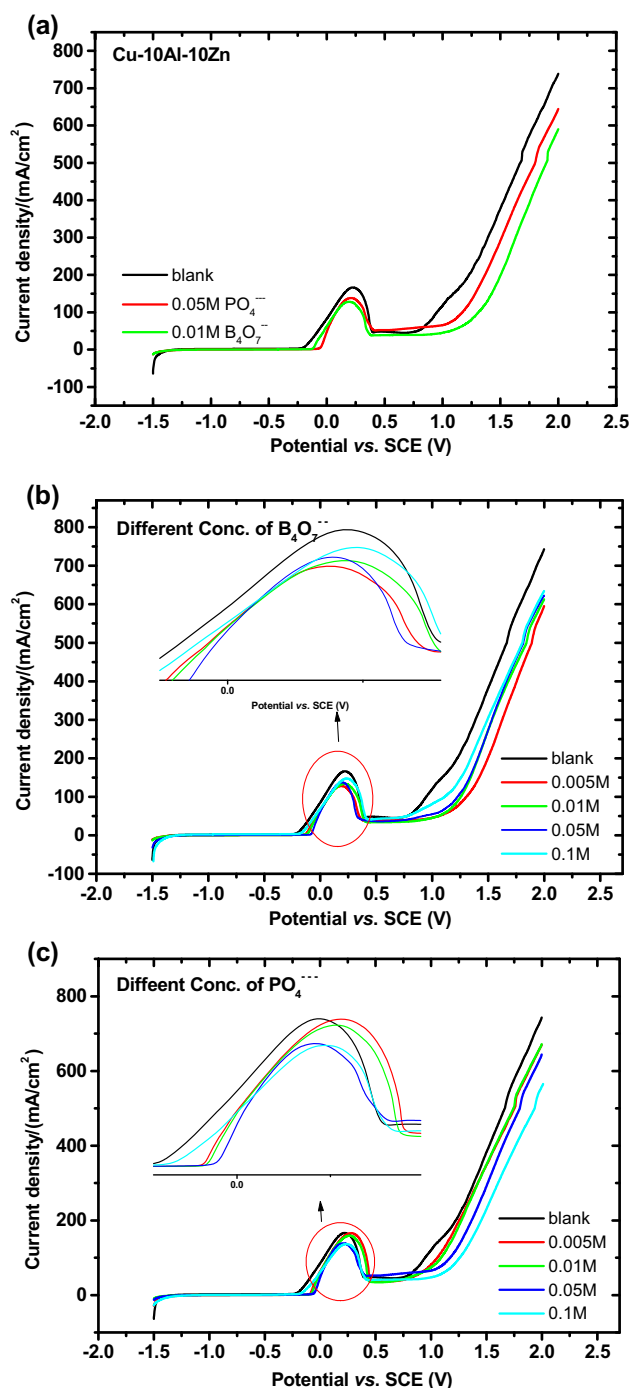

Fig. 2 Anodic potentiodynamic polarization curves for Cu–10Al–10Zn alloy in **a** 3.5% NaCl solution in the absence and the presence of 0.05 M Na_3PO_4 and 0.01 M $Na_2B_4O_7$ at 25 °C, **b** 3.5% NaCl solution containing different concentrations of $B_4O_7^-$, and **c** 3.5% NaCl solution containing different concentrations of PO_4^- at 25 °C

3.2 Linear Potentiodynamic Curves

In this series of experiments, the anodic potentiodynamic polarization curves were recorded for the Cu–10Al–10Zn alloy in 3.5% NaCl solution in the absence (blank) and the

presence of $Na_2B_4O_7$ and Na_3PO_4. The (E/i) curves were swept starting from -1500 mV (SCE) with a scan rate of 10 mV s^{-1} up to $+2000$ mV. Typical anodic curves for the Cu–10Al–10Zn alloy in stagnant naturally aerated 3.5% NaCl solution in absence and presence of 0.01 M Na_3PO_4 and 0.01 M $Na_2B_4O_7$ at pH 9.5 are depicted in Fig. 2a. A transition region before active metal dissolution in which the current density stabilizes with potential was recorded. This transition region is most probably due to the formation of intermediate species such as $CuCl_{ads}^-$ on the electrode surface [26]. The solubility of $CuCl_{ads}^-$ is low, and hence it precipitates at the surface of the electrode forming a porous CuCl film [27]. In the anodic region, a clear anodic peak appears at ~ 250 mV where the current density increases rapidly as the potential increases due to the formation of soluble $CuCl_2^-$ from the dissolution of the adsorbed layer or the dissolution of copper itself [28]. It was suggested that the presence of a high concentration of $CuCl_2^-$ at the metallic surface leads to a hydrolysis reaction and the formation of Cu_2O [29]. The formation of Cu_2O as an insoluble passive layer explains the decrease of anodic current density to a small value known as the passive current density indicating the onset of passivation. The passive current extends up to a certain potential depending on the electrolyte concentrations, other additives, and the alloying elements. As the electrode potential exceeds, a sudden increase in the current density is observed, indicating passivity breakdown, initiation, and propagation of pitting corrosion. The potential value was referred to as pitting potential, E_{pit} [30], when the sudden increase in current density was observed after the passive region. As shown in Fig. 2a, the results reveal that the presence of inorganic additives, 0.01 M PO_4^{3-} and 0.01 M $B_4O_7^{2-}$, shifts the pitting potential, E_{pit}, to more positive values. This means that Cu–10Al–10Zn alloy is more susceptible to pitting corrosion in 3.5% NaCl solution than in the presence of inorganic additives. Also the height of the anodic peak decreased in the presence of the inorganic additives. Figure 2b, c shows the anodic curves for Cu–10Al–10Zn alloy in 3.5% NaCl solution and 3.5% NaCl containing different concentrations of the inorganic additives at 25 °C. The pitting potentials slightly shift to negative values as the $B_4O_7^{2-}$ concentrations increase, but still more positive values were recorded than those recorded in the case of the blank (cf. Fig. 2b). However, the pitting potentials shift to more positive values as the PO_4^{3-} concentrations increased (cf. Fig. 2c). Generally, it can be seen from Fig. 2b that the increase of the borax content ($B_4O_7^{2-}$) causes an increase in the current density values of the anodic peak and at the same time these peaks are still less than those observed in case of
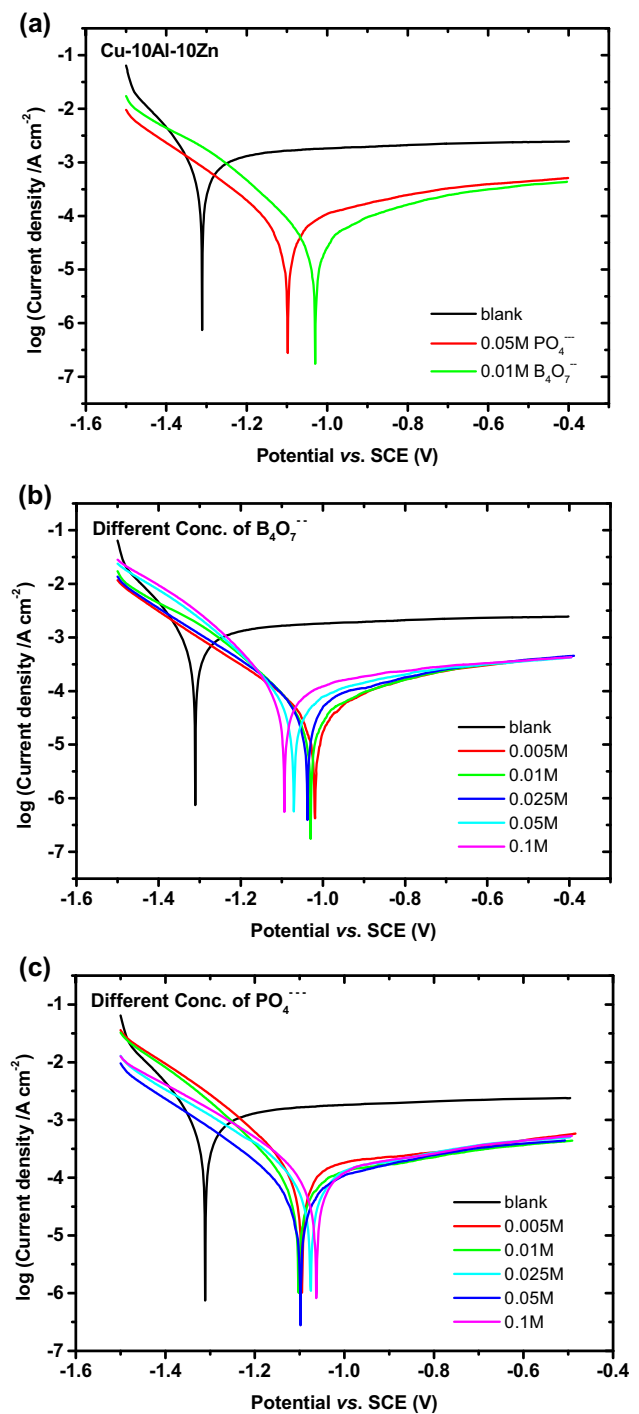
Fig. 3 Polarization curves for Cu–10Al–10Zn alloy after 1 h of electrode immersion in **a** 3.5% NaCl solution in the absence and the presence of 0.05 M Na_3PO_4 and 0.01 M $Na_2B_4O_7$ at pH 9.5 and 25 °C, **b** 3.5% NaCl solution containing different concentrations of $B_4O_7^-$ at pH 9.5 and 25 °C, and **c** 3.5% NaCl solution containing different concentrations of PO_4^- at pH 9.5 and 25 °C

Table 1 Corrosion parameters and inhibition efficiency for Cu–10Al–10Zn alloy in 3.5% NaCl solution in the absence and the presence of different concentrations of PO_4^- and $B_4O_7^-$ at pH 9.5 and 25 °C

Additive	Conc. (M)	E_{corr} (mV)	i_{corr} (μA cm^{-2})	β_a (mV dec^{-1})	β_c (mV dec^{-1})	Corr. rate (mm year^{-1})	Inhibition efficiency
3.5% NaCl	–	−1308	311	122	−74.4	3.80	–
Na$_2$B$_4$O$_7$	0.005	−1015	27.4	134	−119	0.32	91.1
	0.010	−1025	24.8	103	−112	0.30	92.0
	0.025	−1033	29.0	157	−130	0.34	90.5
	0.050	−1067	33.6	189	−102	0.40	89.0
	0.100	−1090	49.1	203	−97	0.57	84.2
	0.200	−1122	56.0	251	−101	0.69	81.8
Na$_3$PO$_4$	0.005	−1091	77.6	248	−112	0.95	75.0
	0.010	−1099	54.8	216	−134	0.67	82.3
	0.025	−1071	423	129	−116	0.51	86.4
	0.050	−1094	20.5	174	−117	0.26	93.4
	0.100	−1059	47.6	185	−118	0.57	84.7
	0.200	−1082	58.4	164	−130	0.70	81.2

the blank. In contrast to Fig. 2c, where the increase of phosphate content (PO_4^{3-}) causes a decrease in the current density values of the anodic peak.

3.3 Corrosion Rate Measurements

Polarization curves were recorded for Cu–10Al–10Zn alloy after 1 h of electrode immersion in stagnant naturally aerated solutions. For comparison, the best inhibitive effects obtained by the inorganic additives are demonstrated in Fig. 3a. This figure shows the representative polarization curves of Cu–10Al–10Zn alloy, measured after reaching the steady state, in 3.5% NaCl and 3.5% NaCl containing 0.01 M Na$_2$B$_4$O$_7$ and 0.05 M Na$_3$PO$_4$ solutions. It is clear that the presence of $B_4O_7^{2-}$ and PO_4^{3-} in the electrolyte shifts the steady-state potential of the alloy to the positive potentials, which can be attributed to a decrease in the rate of anodic reaction. Accordingly, the anodic reaction is inhibited to a larger extent than the cathodic reaction, meaning that these additives act as anodic inhibitors. It is noticed that the recorded open circuit potential is less negative than the corrosion potential recorded in the potentiodynamic polarization measurements. These differences can be attributed to the prepassivation of the alloy surface, where the alloy surface is covered by a passive layer directly after electrode immersion in the aqueous solution. The thickness of the passive layer increases with time, especially in stagnant solutions. This leads to a shift of the steady-state potential in the positive region [31]. The corrosion parameters of Cu–10Al–10Zn alloy, corrosion potential, E_{corr}, corrosion current density, i_{corr}, and both Tafel slopes (anodic, β_a, and cathodic, β_c, peaks) were calculated and are presented in

Table 1. In the absence of inorganic additives, a significant change in corrosion current density was observed, and the corrosion current density reached its maximum value, while it dropped to its minimum value in the presence of 0.01 M Na$_2$B$_4$O$_7$ and 0.05 M Na$_3$PO$_4$, respectively.

The effect of different concentrations of borate and phosphate anions on the polarization curves was investigated and is depicted in Fig. 3b, c. In all cases, the electrode exhibits the same curve shapes similar to that reported previously by the blank. Generally, the corrosion potential shifted to more positive values at lower concentrations and then slightly to negative values as the borate concentration increased and to positive values as the phosphate concentration increased. The calculated inhibition efficiency (IE) and the corrosion parameters for Cu–10Al–10Zn alloy as a function of borate and phosphate concentrations is presented in Table 1. The E_{corr} values here may be somewhat different from the steady-state OCP values shown in Fig. 1a, b probably due to partial removal of the passive film as polarization scanning was started at more negative potential relative to the steady-state potential. In case of borate, the corrosion current density reached a minimum value (24.8 μA cm^{-2}) only at 0.01 M and then increased again till 0.2 M, whilst the current density firstly decreased as the concentration of phosphate increased, reaching a minimum value (20.5 μA cm^{-2}) at 0.05 M, and after that the current density increased again as the phosphate concentration increased from 0.05 to 0.2 M. These results suggest that these anions are acting as corrosion inhibitors for Cu–10Al–10Zn alloy in chloride media, where the inhibition efficiency, IE, reaching the maximum values of 92.0 and 93.4% at 0.01 M $B_4O_7^{2-}$ and 0.05 M PO_4^{3-}, respectively. The inhibitive effect of these anions
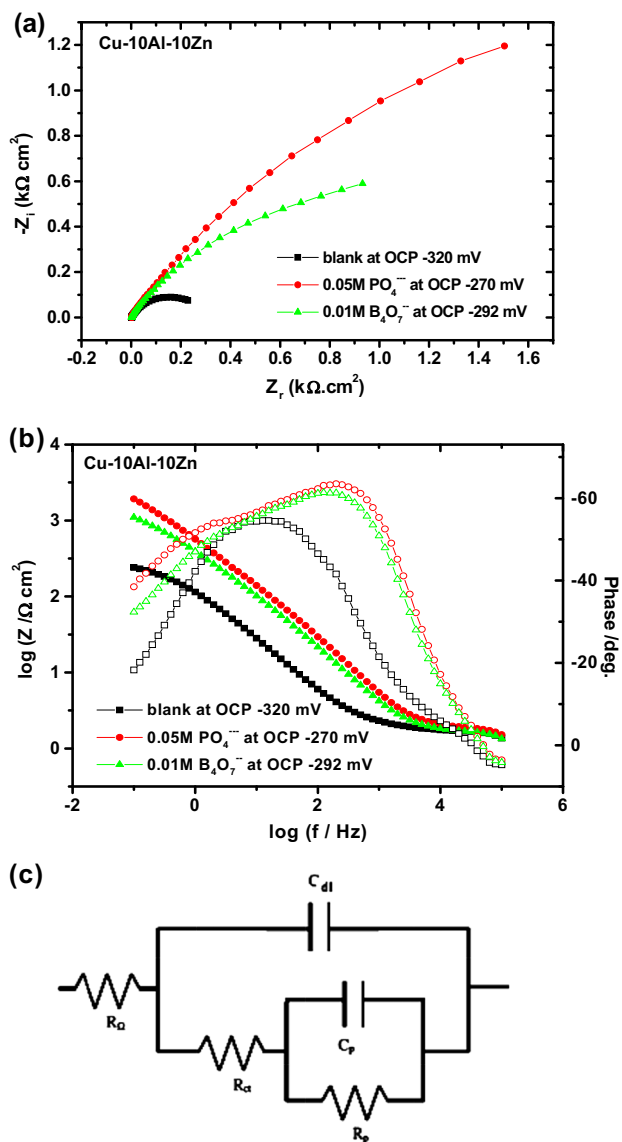
(a)

(b)

(c)

Fig. 4 **a** Bode and **b** Nyquist plots for Cu–10Al–10Zn alloy after 60 min of electrode immersion in 3.5% NaCl solution in the absence and the presence of 0.05 M Na_3PO_4 and 0.01 M $Na_2B_4O_7$ at 25 °C. **c** Equivalent circuit model used in the fitting of impedance data of Cu–10Al–10Zn alloy under different conditions; R_s = solution resistance, R_{ct} = charge transfer resistance, C_{dl} = double-layer capacitance, R_{pf} = passive film resistance, and C_{pf} = passive film capacitance. (filled square) blank at OCP −320 mV, (filled circle) 0.05 M Na_3PO_4 at OCP −320 mV, and (filled triangle) 0.01 M $Na_2B_4O_7$ at OCP −320 mV

can be explained on the basis of the competitive adsorption between these anions and the aggressive Cl^- ions on the passive electrode surface and thus retards their corresponding destructive action [31]. The inhibitive anions may be incorporated into the passive layer on the alloy surface, forming an improved stability against the aggressive ions. The passivating properties of phosphate anions are directly dependent on the pH of the solution, where an increase in

the concentration of Na_3PO_4 is accompanied by an increase in the pH and consequently an increase in the stability of the obtained passive film.

3.4 Electrochemical Impedance Spectroscopy

Further mechanistic information concerning the steady-state corrosion behavior of Cu–10Al–10Zn alloy can be obtained from the pattern of the impedance diagrams, where EIS has been extensively used for studying the formation and properties of the passive film formed on the alloy surface. The impedance data were recorded after 60 min of electrode immersion in stagnant naturally aerated 3.5% NaCl and 3.5% NaCl containing borate and phosphate solutions in the form of Nyquist and Bode plots at pH 9.5 and 25 °C. The impedance spectra of the Cu–10Al–10Zn alloy were recorded at the corresponding steady-state potentials. Figure 4a demonstrates the open circuit impedance complex diagrams (Nyquist plot) for Cu–10Al–10Zn in 3.5% NaCl and 3.5% NaCl containing 0.01 M $B_4O_7^{2-}$ and 0.05 M PO_4^{3-} solutions. The impedance diagram shows two overlapped semicircles, indicating that the corrosion reaction at the Cu–10Al–10Ni electrode is influenced by both charge transfer and mass transport processes. The diameter of each of the two semicircles increases with the presence of $B_4O_7^{2-}$ and PO_4^{3-} ions, and, at a given time, the diameter of the second semicircle is greater than that of the first semicircle. This indicates that the corrosion process is controlled mainly by the second time constant in the low-frequency region. Bode plot format enables equal presentation of impedance data and the appearance of the phase angle as a sensitive parameter for any interfacial phenomena. Therefore, there are two phase maxima that become closer and overlapped as presented in Fig. 4b. The two phase maxima locate at high and low frequency ranges representing the electrode processes. Also, it is worthwhile to mention that the total impedance magnitude of the alloy in the presence of PO_4^{3-} is greater than that in the presence of 0.01 M $B_4O_7^{2-}$. The impedance data were analyzed using the software provided with the impedance system where the dispersion formula was used. For a simple equivalent circuit model consisting of a parallel combination of a capacitor, C_{dl}, and a resistor, R_{ct}, in series with a resistor, R_s, representing the solution resistance, the electrode impedance, Z, is represented by the mathematical formulation:

$$Z = R_s + [R_{ct}/1 + (2\pi f R_{ct} C_{dl})^\alpha], \qquad (1)$$

where α denotes an empirical parameter ($0 \leq \alpha \leq 1$) and f is the frequency in Hz [32, 33]. To account for the presence of a passive film, the impedance data were analyzed using the equivalent circuit model shown in Fig. 4c where another combination R_{pf} and C_{pf} representing the passive

Table 2 Equivalent circuit parameters for Cu–10Al–10Zn alloy in 3.5% NaCl solution in the absence and the presence of different concentrations of PO_4^- and $B_4O_7^-$ at pH 9.5 and 25 °C

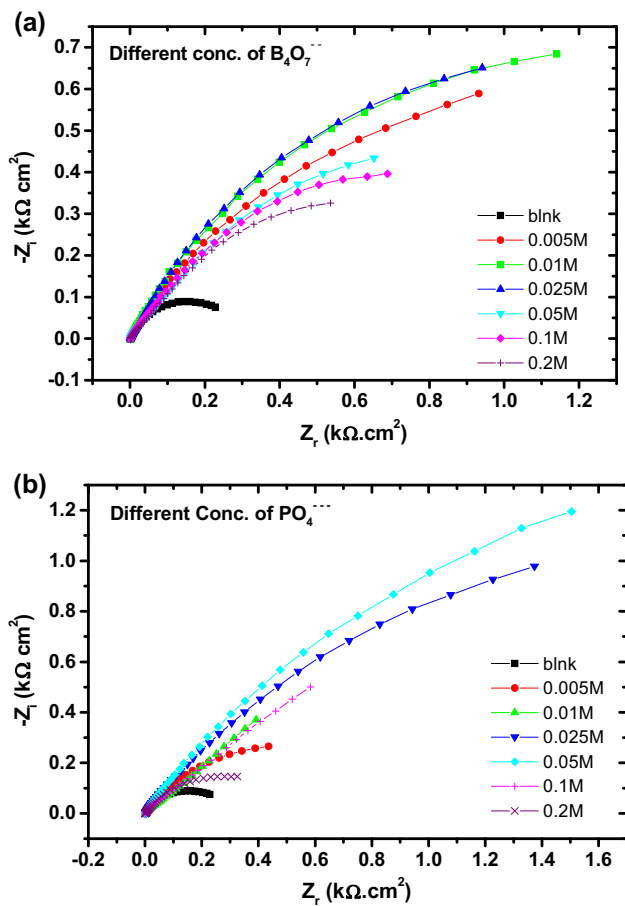| Additive	Conc. (M)	R_s (Ω)	R_{ct} (kΩ cm^2)	C_{dl} (μF cm^{-2})	α_1	R_{pf} (kΩ cm^2)	C_{pf} (μF cm^{-2})	α_2
3.5% NaCl	–	1.50	0.222	102	1.00	0.312	1500	0.99
Na$_2$B$_4$O$_7$	0.005	1.21	0.635	43.1	0.99	2.27	720	1.00
	0.010	1.41	1.390	36.1	0.99	2.55	624	1.00
	0.025	1.52	1.350	24.4	0.99	2.32	685	1.00
	0.050	1.63	0.584	108	0.99	1.63	977	0.99
	0.100	1.51	0.520	61.1	0.99	1.19	1138	1.00
	0.200	1.57	0.361	88.3	0.99	0.931	1370	1.00
Na$_3$PO$_4$	0.005	1.01	0.482	66.1	0.99	0.960	1340	1.00
	0.010	1.12	0.851	50.5	0.99	2.81	750	0.99
	0.025	1.22	1.190	42.1	0.99	4.01	395	1.00
	0.050	1.13	1.630	30.7	0.99	5.32	299	1.00
	0.100	1.31	0.762	113	0.99	3.61	431	1.00
	0.200	1.40	0.399	63	0.99	0.786	1650	1.00

Fig. 5 Nyquist plots for Cu–10Al–10Zn alloy after 60 min of electrode immersion in 3.5% NaCl solution in the absence and the presence of different concentrations of $B_4O_7^-$ (**a**) and different concentrations of PO_4^- (**b**) at 25 °C
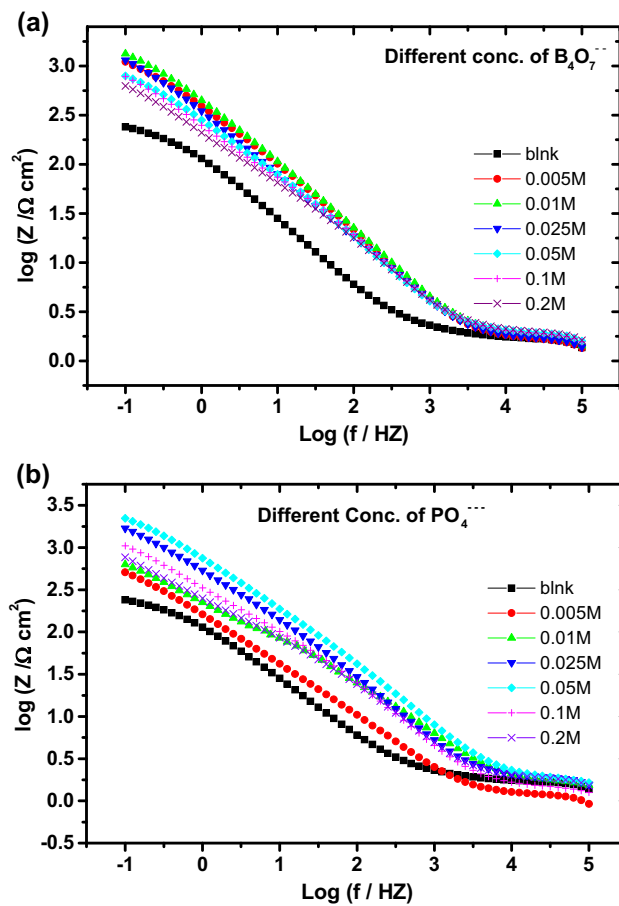
Fig. 6 Variation of total impedance with frequency for Cu–10Al–10Zn alloy after 60 min of electrode immersion in 3.5% NaCl solution in the absence and the presence of different concentrations of $B_4O_7^-$ (**a**) and different concentrations of PO_4^- (**b**) at pH 9.5 and 25 °C
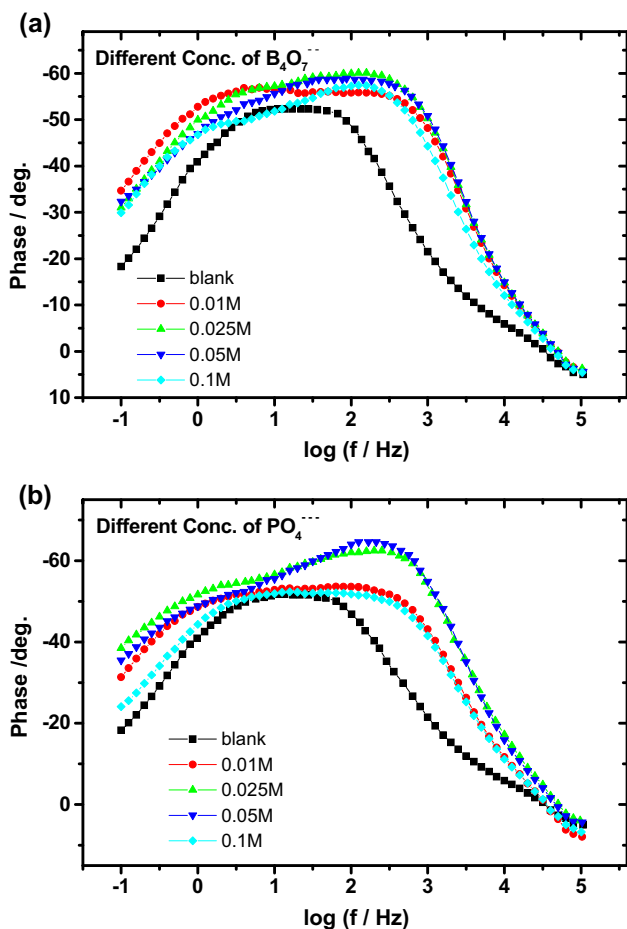
Fig. 7 Variation of phase angle with frequency for Cu–10Al–10Zn alloy after 60 min of electrode immersion in 3.5% NaCl solution in the absence and the presence of different concentrations of $B_4O_7^-$ (a) and different concentrations of PO_4^- (b) at pH 9.5 and 25 °C
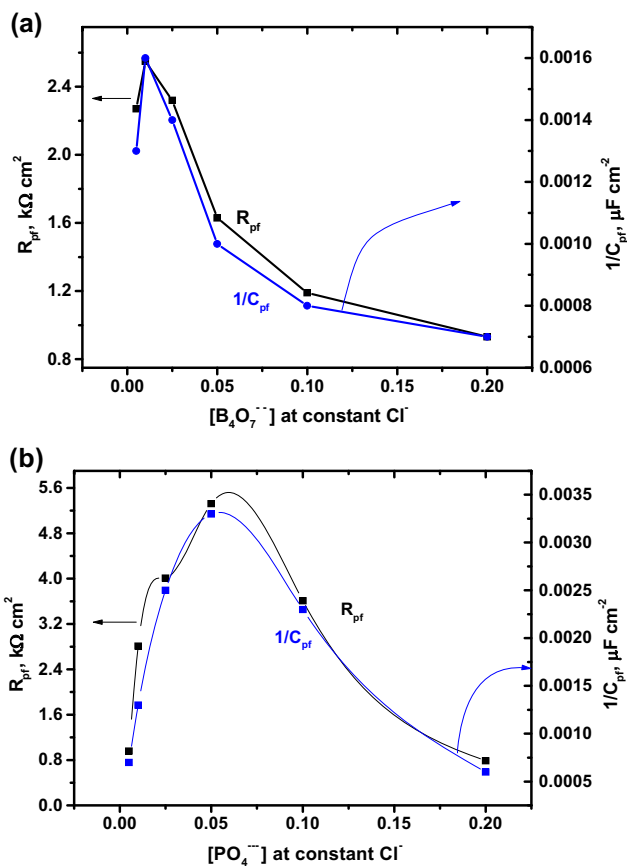

Fig. 8 Variation of passive film resistance, R_{pf}, and relative film thickness, $1/C_{pf}$, formed on the alloy surface with different concentrations of $B_4O_7^-$ (a) and different concentrations of PO_4^- (b) in 3.5% NaCl solution at pH 9.5 and 25 °C

film resistance, R_{pf}, and the passive film capacitance, C_{pf}, was introduced. The calculated equivalent circuit parameters for Cu–10Al–10Zn alloy are summarized in Table 2. The results showed that tri-sodium phosphate has the evident large effect on the corrosion resistance of the alloy than di-sodium tetra-borate, where in the presence of phosphate ions $Zn_3(PO_4)_2$ and $Cu_3(PO_4)_2$ were shown to precipitate on the alloy surface [34, 35].

The influence of the concentrations of borate and phosphate ions on the corrosion process of Cu–Al–Zn alloy was investigated using electrochemical impedance spectroscopy. Figure 5 shows Nyquist plots for Cu–10Al–10Zn alloy after 60 min of electrode immersion in 3.5% NaCl solution in the absence and the presence of different concentrations of $B_4O_7^{2-}$ and PO_4^{3-} at pH 9.5 and 25 °C. It can be seen from this figure that the diameter of impedance loop increased as PO_4^{3-} concentration increased and started to decrease again at 0.05 M PO_4^{3-}, while only 0.01 M

$B_4O_7^{2-}$ was sufficient to achieve the maximum effect and started to decrease again. Figure 6 explains the variation of total impedance with frequency for Cu–10Al–10Zn alloy in 3.5% NaCl solution in the absence and the presence of different concentrations of $B_4O_7^{2-}$ and PO_4^{3-}, where the magnitude of the total impedance at higher frequency increased and started to decrease again. The fitting results are listed in Table 2. In the presence of TSP, the values of R_{ct} and R_{pf} increased with the increasing TSP concentration, extending to a maximum value at 0.05 M. Above this concentration, their values decreased again, possibly due to the formation of looser copper phosphate and zinc phosphate layers resulting from the higher nucleation rates of copper phosphate and zinc phosphate at higher TSP concentrations [36, 37]. Meanwhile, in the case of borax, the R_{ct} and R_{pf} values reach their maximum limits at 0.01 M and decrease with the increase in borate concentration. This behavior indicates that spontaneously grown film on the alloy surface is liable to dissolve in high borate concentration. It is thus evident that dilute borate solutions (cf.
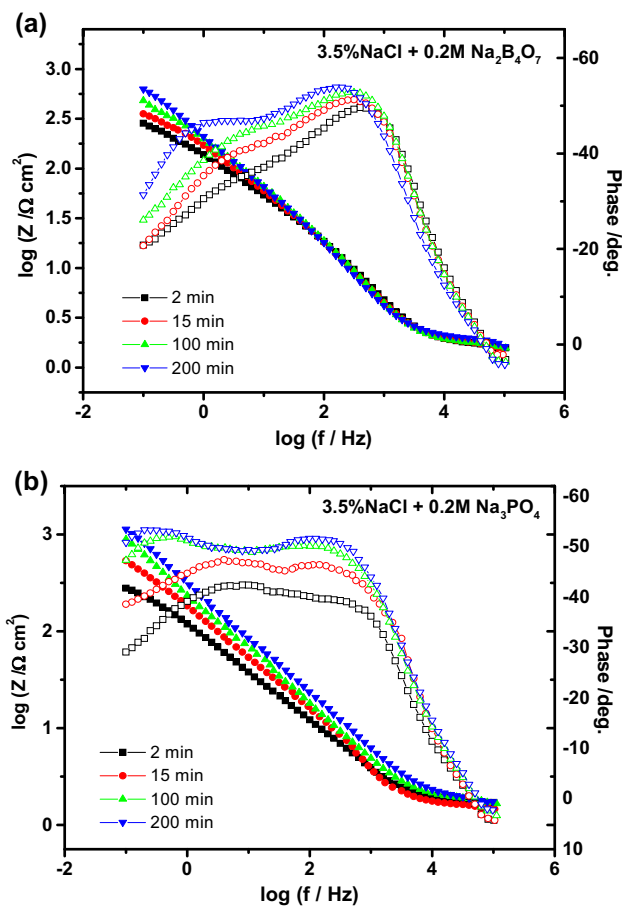
Fig. 9 Bode plots for Cu–10Al–10Zn alloy after different immersion times in 3.5% NaCl + 0.2 M $Na_2B_4O_7$ (**a**) and 3.5% NaCl + 0.2 M Na_3PO_4 (**b**) at pH 9.5 and 25 °C

Fig. 10 Variation of passive film resistance, R_{pf}, and relative film thickness, $1/C_{pf}$, formed on the alloy surface with time in stagnant naturally aerated 3.5% NaCl + 0.2 M $Na_2B_4O_7$ and 3.5% NaCl + 0.2 M Na_3PO_4 at pH 9.5 and 25 °C

Figs. 5a and 6a) offer better conditions for forming surface films with higher protection efficiency, due to the growth of a much thicker and less defective film on the surface. Variation of the phase angle with frequency for Cu–10Al–10Zn alloy in 3.5% NaCl solution in the absence and the presence of different concentrations of TSP and borate is illustrated in Fig. 7a, b. There are two phase maxima at intermediate and high frequencies. The phase maximum in
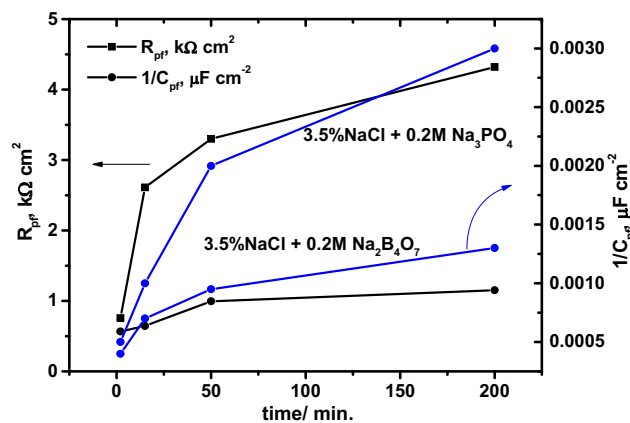
the intermediate frequency range corresponds to the electrical double layer, while that appearing in the low frequency range was attributed to the protective passive film, where the phase maximum decreases at higher concentrations. Since the relative thickness of the passive layer is presented as $1/C_{pf}$ [38]. Figure 8a, b shows, respectively, the variations of the relative passive layer thickness, $1/C_{pf}$, and the passive layer resistance R_{pf}, formed on the alloy surface with different $B_4O_7^{2-}$ and PO_4^{3-} concentrations. The passive film thickness and resistance increase gradually with the increasing anion concentration of $B_4O_7^{2-}$ till 0.01 M and that of PO_4^{3-} till 0.05 M; then they started to decrease again, became thinner, less resistive, and decreased sharply with the increasing anion concentrations. This means that more protective and much thicker films formed on the alloy surface at higher concentrations of TSP than borate.

Figure 9a, b demonstrates the impedance spectra of Cu–10Al–10Zn alloy after different exposure times in the form of Bode plot in 3.5% NaCl + 0.2 M $Na_2B_4O_7$ and 3.5% NaCl + 0.2 M Na_3PO_4. The initial impedance (Z) recorded 5 min after electrode immersion increases as the time of

Table 3 Equivalent circuit parameters for Cu–10Al–10Zn alloy after different times of immersion in 3.5% NaCl solution containing 0.2 M Na_3PO_4 and 0.2 M $Na_2B_4O_7$ at pH 9.5 and 25 °C

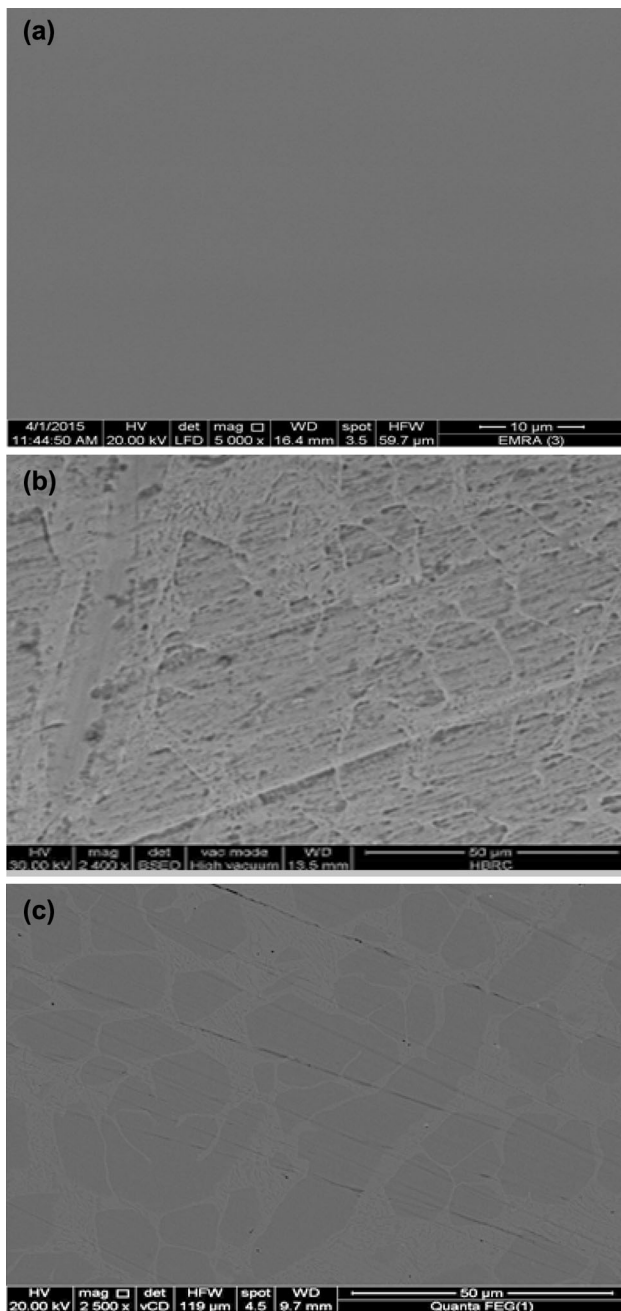| Time (min)	R_s (Ω)	R_{ct} (kΩ cm²)	C_{dl} (μF cm⁻²)	$α_1$	R_{pf} (kΩ cm²)	C_{pf} (μF cm⁻²)	$α_2$
3.5% NaCl + 0.2 M $Na_2B_4O_7$							
2	1.25	0.171	152	1.00	0.565	2500	0.99
15	1.31	0.270	118	0.99	0.644	1450	0.99
50	1.45	0.401	88	0.98	0.995	1100	1.00
200	1.32	0.552	79	0.98	1.150	750	1.00
3.5% NaCl + 0.2 M Na_3PO_4							
15	1.63	0.304	108	0.95	2.61	670	1.00
50	2.01	0.695	91.4	0.99	3.30	450	1.00
200	1.92	0.597	84.2	0.99	4.32	295	0.99

Fig. 11 a SEM micrograph of mechanically polished Cu–10Al–10Zn alloy, **b** after 10 h of immersion in naturally aerated 3.5% NaCl solution, **c** after 10 h of immersion in 3.5% NaCl containing 0.05 M PO_4^{3-} solution

electrode immersion increases. The increase of the impedance values is due to the progressive formation of the passive film on the alloy surface with time. The Bode plots of alloys show two distinguishable phase maxima closer to each other, indicating the presence of two time constants representing the electrode processes. There is more broadening of the phase maximum with the increase in the immersion time reaching the passive behavior [38]. The

equivalent circuit parameters for the alloy at different intervals are summarized in Table 3. In general, the passive film resistance, R_{pf}, and the charge transfer resistance, R_{ct}, increases with the increase of immersion time. Figure 10 presents the variation of corrosion resistance of the barrier layer, R_{pf}, formed on the Cu–10Al–10Zn alloy with the time of immersion in 3.5% NaCl + 0.2 M $Na_2B_4O_7$ and 3.5% NaCl + 0.2 M Na_3PO_4. It is evident that the passive film resistance, R_{pf}, increases with time until a steady state is achieved, and the passive film resistance, R_{pf}, formed on Cu–10Al–10Zn alloy in the case of TSP is remarkably higher than that formed in case of borate. This indicates that PO_4^{3-} is more efficient than $B_4O_7^{2-}$ in the inhibition of the Cu–10Al–10Zn alloy, which is in good agreement with the potentiodynamic polarization results.

3.5 Surface Analyses

SEM analyses were used to define the morphology of the surface attack. So that it essential to see what is happening to the alloy surface before and after the addition of the inorganic inhibitor. Figure 11a presents the SEM micrograph of mechanically polished Cu–10Al–10Zn alloy. The main characteristic of this figure is that the electrode surface appears clearly smooth. After 10 h of immersion in a stagnant naturally aerated neutral 3.5% NaCl solution, more rough, clear corrosion sites can be identified on SEM images presented in Fig. 11b. It is clear that the chloride-containing solution is remarkably aggressive to the electrode surface as can be seen in the SEM image, where the corrosion sites become aggressive at the boundary phases. The presence of the inorganic additives in the corrosive medium leads to the repair of the flawed regions. Figure 11c presents the SEM micrographs obtained after 10 h of immersion in the same solution in the presence of 0.05 M TSP. It is clear that the alloy surface is improved, the flawed regions repaired, and the surface of boundary phases appeared smooth.

4 Conclusions

Phosphates and borates can be considered as effective corrosion inhibitors for the corrosion of the Cu–10Al–10Zn alloy in 3.5% NaCl solution. The presence of the two inorganic additives shifts the steady-state potential of the alloy toward more positive values, indicating that these additives act as anodic inhibitors. The presence of PO_4^{3-} creates protective films on the metal surface that suppress anodic dissolution than $B_4O_7^{2-}$ in 3.5% NaCl solution. The current density decreased as the phosphate concentration increased, reaching a minimum value at 0.05 M PO_4^{3-}, and then increased again, while, in case of borate, the

current density reached a minimum value only at 0.01 M $B_4O_7^{2-}$, but it was higher than that recorded at 0.05 M PO_4^{3-} and then started to increase again. This means that more protective and much thicker film formed on the alloy surface in case of tri-sodium phosphate. For industrial applications, it is recommended to use tri-sodium phosphate as a corrosion inhibitor for Cu–10Al–10Zn alloy in seawater solution.

References

1. Shifler DA (2005) Corros Sci 47:2335
2. Allam NK (2007) Appl Surf Sci 253:4570
3. Bahadur A (1998) Can Metall Q 37:459
4. Yohai L, Schreiner WH, Vázquez M, Valcarce MB (2013) Mater Chem Phys 139:817
5. Coutinho CFB, Silva MO, Machado SAS, Mazo LH (2007) Appl Surf Sci 253:3270
6. Refaey SAM, Abd El Malak AM, Abdel-Fatah HTM, Taha F (2007) Int J Electrochem Sci 2:563
7. El-Tantawy YA, Al-Kharafi FM, Katrib A (1981) J Electroanal Chem 125:321
8. Drogowska M, Brossard L, Menard H, Lasia A (1988) Surf Coat Technol 34:401
9. Souissi N, Triki E (2007) J Mater Sci 42:3259
10. Sayed SM, Ashour EA, Ateya BG (1994) Corros Sci 36:221
11. Goh KH, Lim TT, Chui PC (2008) Corros Sci 50:918
12. Hernandez Creus A, Souto RM, GonZalez S, Laz MM, Salvarezza RC, Arvia AJ (1994) Appl Surf Sci 81:387
13. Yohai L, Vazquez M, Valcarce MB (2011) Corros Sci 53:1130
14. Ashour EA, Ateya BG (1995) Corros Sci 37:371
15. Yohai L, Schreiner WH, Vazquez M, Valcarce MB (2011) Appl Surf Sci 257:10089
16. Valcarce MB, Vazquez M (2010) Corros Sci 52:1413
17. Edwards M, Hidmi L, Gladwell D (2002) Corros Sci 44:1057
18. Pehkonen SO, Palit A, Zhang X (2002) Corrosion 58:156
19. Zhe Y, Pehkonen SO (2004) Water Sci Technol 49:73
20. Li S, Ni L, Sun C, Wang L (2004) Corros Sci 46:137
21. Feng Y, Siow KS, Teo WK, Tan KL, Hsieh AK (1997) Corrosion 53:546
22. Kılınççeker G, Erbil M (2010) Mater. Chem. Phys. 119:30
23. Cai QZ, Wang LS, Wei BK, Liu QX (2006) Surf Coat Technol 200:3727
24. Schmeling EL, Roschenbleck B, Weidemann MH (1990) US Patent 4,978,432
25. Wu CS, Zhang Z, Cao FH, Zhang LJ, Zhang JQ, Cao CN (2007) Appl Surf Sci 253:3893
26. Diard JP, Le Canut JM, Le Gorrec B, Montella C (1998) Electrochim Acta 43:2469
27. Crundwell FK (1991) Electrochim Acta 36:2135
28. Kear G, Barker BD, Stokes K, Walsh FC (2004) J Appl Electrochem 34:659
29. Bacarella AL, Griess JC (1973) J Electrochem Soc 120:459
30. Amin MA, Abd El Rehim SS, Moussa SO, Ellithy AS (2008) Electrochim Acta 53:5644
31. Abel EW (1965) In: Bailar JC et al (ed) Comprehensive inorganic chemistry, vol. 2. Pergamon Press, Oxford, p 124
32. Hladky K, Calow LM, Dawson JL (1980) Br Corros J 15:20
33. Hitzig J, Titz J, Juettner K, Lorenz WJ, Schmidt E (1984) Electrochim Acta 29:287
34. Pickering HW (1983) Corros Sci 23:1107
35. Sillen LG (1964) Stability constants of metal-ion complexes. Special Publications No. 17, The Chemistry Society, London
36. Powell SM, McMurray HN, Worsley DA (1999) Corrosion 55:1040
37. Liu S, Zhong Y, Jiang RY, Zeng ZO, Feng ZP, Xiao R (2011) Corros Sci 53:746
38. Ismail KM, El-Moneim AA, Badawy WA (2001) J Electrochem Soc 148:81